Study into luminescence and photoconductivity of nano-structured ZnO obtained through sol-gel method

IOP Conf. Series: Materials Science and Engineering **597** (2019) 012051 doi:10.1088/1757-899X/597/1/012051

Study into luminescence and photoconductivity of nano-structured ZnO obtained through sol-gel method

L V Mikhnev, E A Bondarenko, O M Chapura*, A A Skomorokhov, A I Nikonov, M S Malorodov, R V Pigulev and D L Gazdinsky

North-Caucasus Federal University, Pushkin Street 1, Stavropol 355009, Russian Federation

*Email: ChapurOL-7@mail.ru

Abstract. Sol-gel method from zinc acetate in water was employed to synthesize nano-sized zinc oxide. The structural features of the ZnO obtained samples, their spectral features of luminescence and photoconductivity were studied. The influence of the treatment temperature on the luminescence and photoconductivity of nano-sized zinc oxide was studied. The type and energy position of the intrinsic defects involved in the luminescence and photoconductivity processes were determined.

1. Introduction

In recent years, a wide range of possible applications of nanomaterials and nanoparticles of zinc oxide in particular has resulted in an interest in their physical and chemical properties. Nanoparticles of zinc oxide themselves and in composites offer potential for the creation of antibacterial agents [1, 2], active materials for toxic waste processing [3], as well as for the detection of fire-hazardous and poisonous gases [4]. Zinc oxide can be used in the ultraviolet range optoelectronic devices while due to the high binding energy of the exciton (60 meV), radiation can be generated at high temperatures reaching 550 K [5]. ZnO nanoparticles can be used in the development of ultraviolet radiation sensors and high-efficiency solar cells [6, 7].

Currently, there are many methods for developing zinc oxide nanostructures, namely – sonochemical [8], sol-gel [9], hydrothermal [10], etc. These methods in combination with the possibilities of varying the synthesis technological parameters make it possible to obtain structures based on ZnO of different morphology. At the same time, the fields of their application are not determined only by the geometric parameters of the nanoparticles, yet also by a set of physical and chemical properties of the resulting group of nanoparticles, while the latter is known to be significantly affected by the defective situation in the synthesized structures.

Most often, the composition of point defects involved in radiative recombination, is successfully evaluated through studying photoluminescence spectra [11-16]. At the same time, the study of photoconductivity spectra allows investigating electronic transitions in a material, including those involving defects that lead to the appearance of free nonequilibrium charge carriers. Therefore, analysis of the luminescence spectra and photoconductivity in a combination stand as a more detailed method for estimating the defect situation.

2. Materials and methods

Zinc acetate dihydrate ($Zn(CH_3COO)_2 \cdot 2H_2O$), 25% ammonia solution ($NH_3 \cdot H_2O$) and distilled water were used as the initial materials for synthesis ZnO nanoparticles. First, a 0.5 M aqueous zinc acetate solution was prepared. To the resulting solution, at intensive stirring, the ammonia solution was added dropwise, with continuous monitoring of the pH level. At pH ≈ 8, the process was stopped, since it is at this acidity value that zinc oxide is formed from its hydroxide. Next, the received gel was centrifuged at 2500 rpm, and the resulting precipitate was triple-washed with distilled water. This procedure is needed to remove various impurity ions remaining after the reaction taking place between zinc acetate and ammonia solution. Further on, the washed gel was dried at a temperature of 110 °C for 12 hours. For the synthesis of experimental samples 1, 2, 3, the powders obtained through drying were subjected to additional thermal treatment at temperatures of 175, 270 and 400 °C, respectively.

The structural features of the obtained particles were studied with X-ray diffraction and scanning electron microscopy, using the PANalytical Empyrean and TESCAN MIRA3 devices, respectively. The measurements of optical, luminescent and photoelectric properties were done on an automated installation based on a monochromator MDR-41 (Lomo JSC). When studying the photoconductivity spectra, the powder was placed in a sandwich-type cell consisting of two quartz glasses with transparent antimony doped tin dioxide electrodes applied. The thickness of the active layer was controlled by fluoroplastic liners and was around 100 μm. Prior to the measurements, the cell with the sample had been kept in the dark for 12 hours.

3. Results and discussion

Figure 1 shows the outcomes of studying the structural features of zinc oxide based nanoparticles obtained via the sol-gel method.

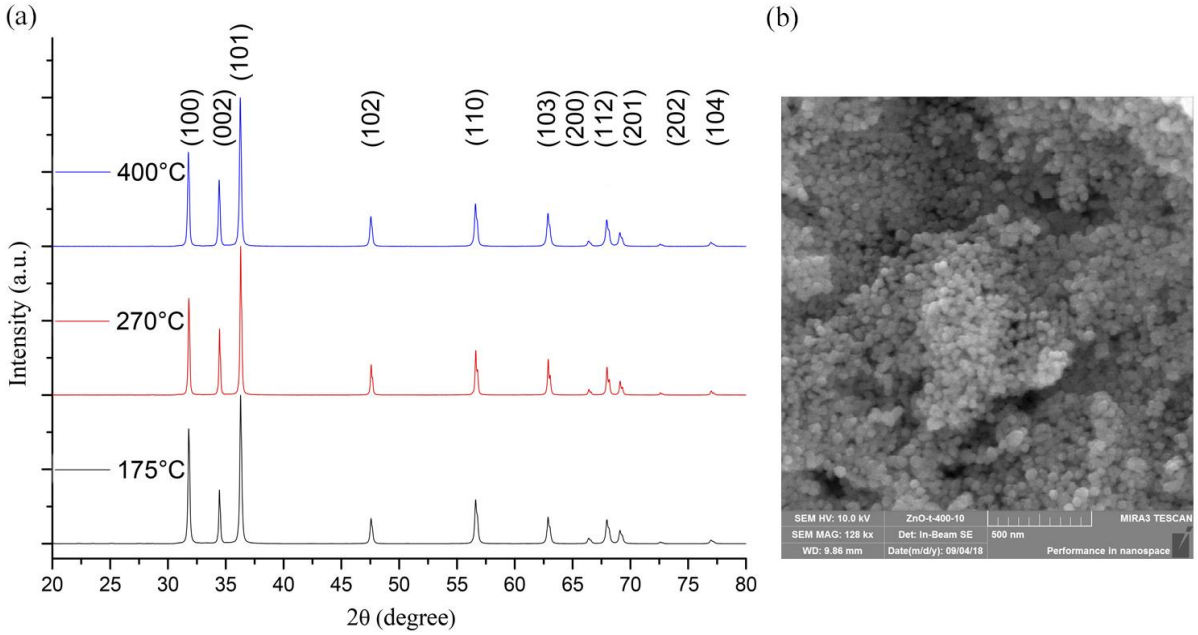

Figure 1. XRD patterns of ZnO samples annealed at different temperatures (a) and an electron microscopic image of a ZnO sample subjected to thermal treatment at a temperature of 400 °C (b).

As can be seen from figure 1, the diffractograms of ZnO samples subjected to thermal treatment at different temperatures, display peaks typical of zinc oxide in wurtzite-type structure (JCPDS card no. 36-1451). Besides, as the calcination temperature increases, the intensity and narrowing of the peaks in the diffractograms do up, which is associated with an increase in ZnO nanoparticles dimensions due to particles aggregation during sintering and improved crystallinity of the resulting samples. The

estimates of the crystallite size, performed using the Debye-Scherrer formula for the (101) plane, yielded the values of 12, 30 and 38 nm for samples 1, 2 and 3, respectively.

As the results of the analysis of electron-microscopic images showed, the obtained zinc oxide nanoparticles have a shape that is close to spherical, figure 1, (b).

The optical band gap (ΔE_g) of nano-sized ZnO was evaluated through studying the diffuse reflection spectra employing the Kubelka-Munk function following the method described in [17], figure 2. The results of the evaluation numerical values can be seen in Table 1.

Table 1. Major features of nano-sized ZnO obtained through sol-gel method.

# of sample	T_{samp}, C	ΔE_g, eV	The average particle size, nm
Sample 1	175	3.45	12
Sample 2	270	3.29	30
Sample 3	400	3.27	38

The displacement of the absorption edge into the region of lower energies (observed from diffuse reflection spectra), and hence the width of the band gap, along with increasing processing temperature is associated with an increase in the size of the ZnO nanoparticles [18,19].

The luminescence spectra were measured at excitation into the fundamental absorption region with 3.96 eV quanta (the band excreted by a monochromator from the spectrum of a high-pressure mercury lamp was used as the source of excitation).

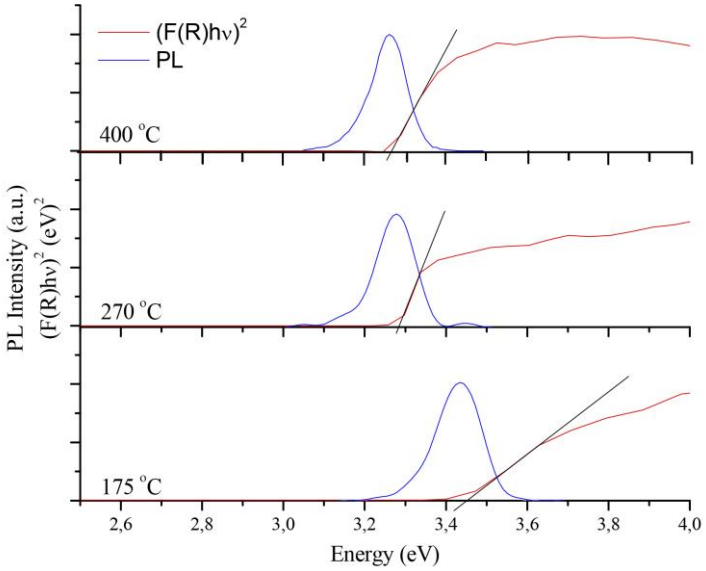

Figure 2. Tauc plots ($(F(R)h\nu)^2$) and spectra of edge photoluminescence (PL) of nanoparticles ZnO.

All the samples had luminescence in two non-overlapping ultraviolet and visible spectral regions. In the ultraviolet region, this was the edge luminescence (figure 2, curves b), where the presence of ZnO is explained by radiative recombination of free excitons [5,11]. Note to be made that the position of the luminescence maximum peak basically coincides with the values of ΔE_g obtained when analyzing the diffuse reflection spectra.

The maximum of the edge luminescence spectrum shifts to the long-wave region along with an increase in the processing temperature, which also indicates a decrease in the width of the band gap. The increase in the intensity of this luminescence at increasing temperature can be attributed to improved crystallinity of the samples.

The visible luminescence spectra in figure 3have a non-elementary form and can be decomposed into separate Gaussian components. For all the samples, the luminescence spectra consist of two elementary bands (in figure 3 they are shown as 1 and 2, respectively), whereas there is a change in the contribution magnitude and the maximums position of these bands along with an increase in the processing temperature.

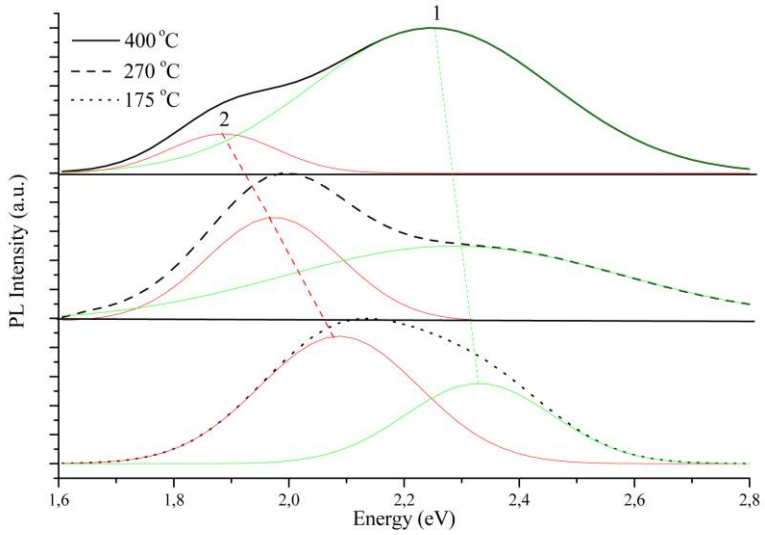

Figure 3. Photoluminescence spectra of nanoparticles ZnO (λ_{ex}=365 nm).

The maximum of luminescent band 1 is located at a wavelength of 530 nm, while its contribution goes up along with an increase in the processing temperature. For band 2, when the sample processing temperature is increased, the maximum is shifted to the long-wave region (for sample 1 the value obtained was 587 nm; for sample 2 – 635 nm; for sample 3 – 642 nm), whereas its contribution to the visible light intensity decreases.

To determine the luminescence and photoconductivity centers, measurements of the photoconductivity spectral features were carried out (figure 4, curves a) and photoexcitation (figure 4, curves b) of nano-sized ZnO. The photoexcitation spectra were measured by recording the radiation at the luminescence maximum.

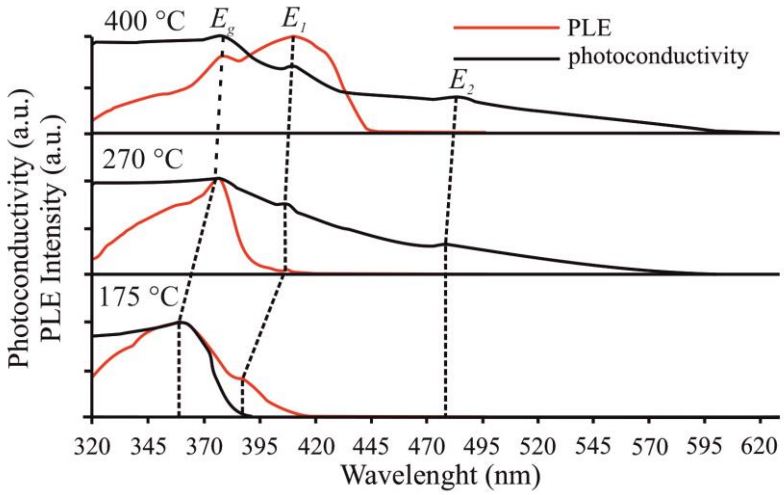

Figure 4. Spectra of photoconductivity and photoexcitation (λ_{em}=530 nm) of nanoparicles ZnO.

At the present time, two reasons have been described for the disturbed current transmission during photoexcitation of powder structures based on zinc oxide. The first reason is due to deep capture levels the presence in ZnO [20], while the second one is related to the effect that adsorbed oxygen has on the conductivity mechanisms [21]. At the same time, we believe that the nature of the current transmission does not have a significant effect on the position of the local maxima in the photoconductivity spectrum.

The figure show that in the photoconductivity and photoexcitation spectra, all the samples reveal typical peaks indicated as E_g and E_1; besides, the photoconductivity spectra for samples 2 and 3 reveal a peak in the 470-490 nm region, which is indicated as E_2.

The E_g peak in its position (Table 2) can be linked to electronic interband transitions. The photoconductivity in the visible region is apparently associated with point defects in zinc oxide, which is also mentioned in [22]. Along with increasing processing temperature, the position of these peaks shifts to the long-wave region; this is well associated with a change in the band gap size. An increase in photoconductivity observed along with an increase in the annealing temperature may be due to the hydroxyl groups desorption from the zinc oxide nanoparticles surface.

Table 2. Major features of photoexcitation and photoconductivity spectra of nano-sized ZnO.

# of sample	Peak E_g		E_1		E_2		Relative photoconductivity value
	nm	eV	nm	eV	nm	eV	
Sample 1	361	3.43	387	3.2	–	–	0.17
Sample 2	375	3.3	407	3.04	479	2.58	0.19
Sample 3	377	3.29	410	3.02	484	2.56	1

When assessing a defective situation, it can be assumed that defects with a low formation energy should prevail. Such defects are vacancies of zinc V_{Zn} and oxygen V_O [19, 24], while at processing temperatures above 200 ˚C other defects [23, 24] should be expected, such as interstitial oxygen atoms O_i, Zinc in the Zn_i interstitium, as well as atoms in anti-structural positions of O_{Zn}, Zn_O. Of all the defects listed above, under abundance of oxygen, Zn_O reveals a very high formation energy [24], so it is unlikely to have a significant effect on zinc oxide photoluminescence and photoconductivity. Zinc in the interstitial Zn_i, as is described in [23], has a very low activation energy for migration, and hence its concentration should be minimal. Therefore, the following defects should be responsible for luminescence and photoconductivity in the obtained samples – zinc V_{Zn} oxygen V_O vacancies and interstitial oxygen atoms O_i, oxygen in the anti-structural position of O_{Zn}.

Since in our case the thermal treatment was carried out in the air atmosphere, the concentration of oxygen vacancies should decrease along with an increase in the temperature due to vacant oxygen sites being filled with adsorbed oxygen atoms. At the same time, the concentration of zinc vacancies should go up due to the release of metal ions to the oxide surface, which in some cases leads to the formation of a metallic phase that delivers the powders gray color.

Given the considerations above, the luminescence band 1, whose intensity increases along with an increasing temperature, can be related to the transition of an electron from the conduction band to the zinc vacancy. A similar energy position was calculated in [25] for the free levels of V_{Zn}^0 and V_{Zn}^{-1}. The luminescence band 2, whose intensity goes down as the annealing temperature increases, can be related to the transition of an electron from the oxygen vacancy to the valence band. The energy position of the free level V_O^{+1}, theoretically calculated in [25], correlates well with the experimental data that we obtained for ZnO sample annealed at temperature of 175 ˚C.

The shift in the second band luminescence maximum is probably associated with a change in the radiative recombination path. As the processing temperature rises, the concentration of oxygen vacancies decreases, while the concentration of defects of another type increases simultaneously, which may be O_i^{-1}, whose recombination, involving the free level, can give red luminescence [26].

An increase in the thermal treatment temperature leads to a significant increase in the contribution that the E_1 peak has to the photoconductivity, and apparently, it can be related to zinc vacancies. In its energy position [25], it coincides with the transition of electrons from the occupied level V_{Zn}^{-1} to the conduction band.

The photoconductivity peak E_2, which can be seen in samples annealed at above 270 ˚C, can be associated with defects of O_i, O_{Zn}. The concentration of interstitial oxygen and zinc atoms in an anti-structural position should go up along with increasing temperature under conditions rich in oxygen, since they perform a compensating role, similar to zinc vacancies [24]. The O_i, and O_{Zn} defects are deep acceptors and the photoconductivity peak E_2 is associated with electron transition from the O_i, O_{Zn} level to the conduction band. Mention to be made that the position of the occupied O_i^{-2} level calculated in [27] fits the data obtained in the data we obtained through our study.

4. Conclusion

The study was aimed at investigating the spectral features of the luminescence and photoconductivity of nano-sized ZnO obtained by the sol-gel method. The outcomes show along with an increase in the processing temperature, the optical width of the band gap decreases, which is probably due to an increase in the crystallite size of zinc oxide nanostructures. The obtained zinc oxide samples proved to have luminescence in the near ultraviolet and visible regions. The luminescence in the ultraviolet region is explained with the appearance of free excitons radiative recombination. The luminescence in the visible region is associated with the recombination of photoexcited charge carriers involving the levels of intrinsic point defects of zinc oxide. Zinc oxide nanostructures were revealed to possess photoconductivity where three characteristic peaks can be distinguished, of which the first one is associated with the interband mechanism of nonequilibrium charge carriers emergence, whereas the second and third ones – with intrinsic defects involved in increasing conductivity upon visible radiation absorption.

Given the results of the impact that the thermal treatment temperature has on the photoluminescence and photoconductivity spectra, possible transitions of charge carriers involving defects levels and allowed bands, were analyzed. Based on this, visible luminescence is associated with electrons transition from the conduction band to the V_{Zn}^{0} and V_{Zn}^{-1} (band 1) vacancies, and from the V_O^{+1} oxygen vacancies to the valence band (band 2). At the same time, an increase in the thermal treatment temperature results in a shift of the 2-band maximum to the long-wave region, associated with the occurrence of recombination involving O_i^{-1} defects. Photoconductivity in the visible region is associated with the occurrence of nonequilibrium charge carriers due to electron transition from the occupied levels of V_{Zn}^{-1} (band E_1) and O_i^{-2}, O_{Zn} (band E_2) to the conduction band.

References

[1] Raghupathi K R, Koodali R T and Manna A C 2011 *Langmuir* **27** 4020–28
[2] Shu Z, Zhang Y, Yang Q and Yang H 2017 *Nanoscale Res. Lett*. 12:135
[3] Hoffmann M R, Martin S T, Choi W and Bahnemannt D W 1995 *Chem. Rev.* **95(1)** 69–96
[4] Hsua C-L, Chenb K-C, Tsaic T-Y and Hsueh T-J 2013 *Sens. and Actuators B:Chemical* **182** 190-196
[5] Özgür Ü, Alivov Y I, Liu C, Teke A, Reshchikov M A, Doğan S, Avrutin V, Cho S-J and Morkoç H 2005 *J. of Appl. Phys*. **98** 041301
[6] Lim J W, Hwang D K, Lim K Y, Kang M, Shin S-C, Kim H-S, Choi W K and Shim J W 2017 *Solar Energy Materials and Solar Cells* **169** 28–32
[7] Fang J, Fan H, Tian H, Dong G 2015 *Mater. Charact.* **108** 51–7
[8] Jung S-H, Oh E, Lee K-H, Yang Y, Park C G, Park W and Jeong S-H 2008 *Cryst. Growth Des*. **8** 26–9
[9] Hayat K, Gondal M A, Khaled M M, Ahmed S and Shemsi A M 2011 *Appl. Catal.* A: General **393** 122–9
[10] Baruwati B, Kumar D K and Manorama S V 2006 *Sensors and Actuators* B: Chemical **119** 676–

82
[11] Djurisic A B, Ng A M C and Chen X Y 2010 *Progress in Quantum Electronics* **34** 191–259
[12] Zhang L, Yin L, Wang C, Lun N, Qi Y and Xiang D 2010 *J. Phys. Chem.* C **114** 9651–8
[13] Li M, Xing G, Xing G, Wu B, Wu T, Zhang X and Sum T C 2013 *Phys. Rev.* B **87** 115309
[14] Kawabata K, Nanai Y,· Kimura S and Okuno T 2012 *Appl Phys.* A **107** 213–20
[15] Camarda P, Messina F, Vaccaro L, Agnello S, Buscarino G, Schneider R, Gerthsen D, Lorenzi R, Gelardi F M and Cannas M 2016 *Phys. Chem. Chem. Phys*. **18** 16237–44
[16] Han N, Wu X, Chai L, Liu H, Chen Y 2010 *Sens. and Actuators* B **150** 230–8
[17] Stone F S 1983 UV-visible diffuse reflectance spectroscopy applied to bulk and surface properties of oxides and related solids *Surface Properties and Catalysis by Non-Metals* ed by J P Bonnelle, B Delmon, E G Derouane (Dordrecht: Springer), chapter 8 pp 237-272
[18] Chithira P R and John T T, 2017 *J. of Luminescence* **185** 212–8
[19] Koao L F, Dejene F B and Swart H C 2014 *Materials Sci. in Semiconductors Process*. **27** 33–40
[20] Nayak J, Kasuya J, Watanabe A and Nozaki S 2008 *J. Phys.: Condens. Matter.* **20** 195222
[21] Prades J D, Hernandez-Ramirez F, Jimenez-Diaz R, Manzanares M, Andreu T, Cirera A, Romano-Rodriguez A and Morante J R 2008 *Nanotechnology* **19** 465501
[22] Mishra S K, Srivastava R K and Prakash S G 2012 *J. Alloys and Comp.* **539** 1–6
[23] Janotti A and Van de Walle C G 2009 *Rep. Prog. Phys.* **72** 126501
[24] Vidya R, Ravindran P, Fjellvag H, Svensson B G, Monakhov E, Ganchenkova M and Nieminen R M 2011 *Phys. Rev.* B **83** 045206
[25] Patterson C H 2006 *Phys. Rev.* B **74** 144432
[26] Lee C T 2010 *Materials* **3** 2218–59
[27] Hu J and Pana B C 2008 *J. Chem. Phys.* **129** 154706